


RESEARCH ARTICLE

Path-following and collision-avoidance guidance of unmanned sailboats based on beetle antennae search optimization

Yingjie Deng¹ , Tao Ni^{2,*}, Zhuxin Zhang² and Jianwei Wang¹

¹School of Mechanical Engineering, Yanshan University, Qinhuangdao 066004, China and ²School of Vehicle and Energy, Yanshan University, Qinhuangdao 066004, China

*Corresponding author. E-mail: nitao@jlu.edu.cn

Received: 14 August 2022; **Revised:** 3 February 2023; **Accepted:** 2 March 2023; **First published online:** 30 March 2023

Keywords: path following, collision avoidance, unmanned sailboat, beetle antennae search

Abstract

There are few studies on the intelligent guidance of unmanned sailboats, which should coordinate pluralistic tasks at sea in the nature of its maneuvering intractability. To ensure the algorithmic practicability, this paper proposes a path-following and collision-avoidance guidance approach of unmanned sailboats with total formulaic description. The risk-detecting mechanism is fabricated by setting a circular detecting zone and using the time to the closest point of approach. Then, the risk of collision, the path deviation, the speed loss, and the course loss can be judged by constructing the cost functions and applying the distance to closest point of approach. The optimized heading angle is deemed as the one minimizing the aggregate cost functions, which is sought by applying and improving the beetle antennae search (BAS) algorithm. In the proposed modified BAS, the searching step is redesigned to enhance the searching efficiency. To ensure the convergence of the real heading angle to the reference, the backstepping-based control law is fabricated for the high-order sailboat model and in the linear form. The control parameters are offline optimized through the modified BAS. Compared with the adaptive control, this controller can guarantee more computation simplicity and the optimized control performance. Finally, simulation corroborates that the sailboat can successfully complete path following and collision avoidance while encountering multiple static and moving obstacles under the proposed schemes.

1. Introduction

The unmanned sailboat is a special marine autonomous surface ship (MASS) propelled by the wind sail rather than the electric motor or the internal-combustion engine. This fact makes it more suitable for long-term and oceangoing tasks in lighter weight and smaller size, such as trophic cyclone monitoring and oceanic data gathering. Moreover, the sailboat can sail silently and serve for military action and marine animal surveillance [1]. Routing, guidance, and control are essential to steer the unmanned sailboats autonomously. However, due to changeable weather and intricate sea environment, steering a sailboat is a challenging issue [2]. Especially, the sailboat must travel by the zigzag leg to prevent its stall in downwind and upwind situations, namely tacking and jibing maneuvers. Ideally, the sailboat should follow the reference path. However, the emergence of obstacles may provoke the contradiction between path following and collision avoidance in the light of security. How to arrange the above tasks simultaneously is worthy of discussion.

To ensure the effective navigation of sailboats in actual sea environment, the real-time routing and guidance approaches are designed and working as a pilot. Routing determines the real-time reference path of the sailboat depending on the meteorological and obstacle information, where guidance directly derives the ideal heading angle and speed of the ship. Current routing outcomes of marine surface crafts learnt much from planar mobile robots, such as the A* algorithm, the potential field method, and

the ship domain method. In refs. [3–5], the meteorological information was incorporated into routing graph, where A* algorithm was employed to calculate the optimal long-term route; ref. [6] proposed a mission programming system, where the new waypoints were created by executing the sequence of actions during the accomplishment of missions; ref. [7] involved wave effect on the speed polar diagram, and the reference path can be decided by the Dijkstra algorithm with a multicriteria objective function. To find the compromise among conflicting objectives, the Pareto-optimal set of routes was made by solving multiobjective optimization problems; for example, routing optimization was proposed with the drifting ice in ref. [8] and the customized constraints in ref. [9]. In ref. [10], an attractor/repellor routing approach of unmanned sailboat was proposed, which provided the possible headings by using an array of waypoint attractors and repellors. In ref. [11], the appropriate reference path of a smart ship can be found by using Q-learning after sufficient training. Nevertheless, there are some mutual limitations in the above routing results. First, routing was all deployed on a graph composed of grids, which implies the limited selections on the ship's directions. Second, the routing method was not highly adaptable to the changeable environment, for example, the coming ships and the erratic weather.

Compared with routing, guidance can directly generate the reference heading direction and speed of the ship, which is more acceptable to the controller. Ref. [12] proposed a velocity-made-good guidance method, where the reference heading angle was to ensure the maximum velocity of the sailboat towards the target. However, this method did not consider collision avoidance. Refs. [13–15] introduced the potential field method to the guidance of unmanned sailboats, where the reference heading angle faced towards the inverse gradient direction by adding up the attractive field of the target and the repulsive fields of wind and obstacles. In ref. [16], the voter-based guidance algorithm was introduced by choosing the maneuver with maximum votes. The above research only considered the waypoint tracking, whereas in nautical practice, path following of great circle routes is most often concerned. For this purpose, the line-of-sight (LOS) guidance was first introduced to unmanned sailboats in ref. [17], where the lane with a fixed width was added to constrain tacking and jibing maneuvers. With the complete mathematical description, the parametric LOS guidance of unmanned sailboats was first proposed in ref. [18], where a sign function described the switching of reference heading angles between tacking and jibing. Concerned with path following of a curved reference path, ref. [19] proposed a parallel guidance algorithm of unmanned wing-sailed catamarans. The above path following guidance of sailboats did not consider collision avoidance. Although there were plenty of outcomes on the collision avoidance of common powered ships, such as the dynamic virtual ship guidance in ref. [20] and the velocity obstacle method in ref. [21], they cannot be applied to the sailboat. Most importantly, the sailboat is not self-propelled, the speed of which strongly relies on the wind. By all accounts, there was seldom research on a uniform guidance framework for the sailboat, which synthesized path following and collision avoidance all together.

According to the separate principle [22], the rudder solely dominates the turning of the sailboat, and the sail can be adjusted in the principle of the maximum speed. With the reference heading provided by the guidance module, the rudder controller is designed to compel the convergence of the actual heading to the reference. In ref. [23], both the rudder and the sail controllers were designed as the fuzzy logic systems (FLS), which were fabricated through the expertise of skippers such that the rollover risk can be eliminated. In refs. [15, 24, 25], the rudder controller was constructed by using PID control, which was classical and easy. However, PID was not adept in dealing with unknown model dynamics. In ref. [26], the \mathcal{L}_1 adaptive control was employed in the Nomoto model of the sailboat, and nice robustness to disturbances was exhibited. In ref. [27], robust control was also achieved by using backstepping with tuning parameters. However, the control performance of robust control relied much on the tuning parameters. How to select optimal parameters was not addressed. In refs. [19, 28], the FLSs were to approximate unknown model dynamics, and event-triggered fuzzy control was fabricated for sailboats. Although the unknown model dynamics can be compensated, these adaptive control was computationally complicated. For the marine crafts cruising in diverse sea environment, it is urgent to strike a balance between adaptability and control conciseness.

Faced with the above challenges, this paper proposed a succinct guidance and control framework of the sailboat. The risk detecting mechanism is fabricated by using time to the closest point of approach (TCPA). Corresponding to various tasks, the cost functions are constructed by complying with the nautical practice and involving distance to closest point of approach (DCPA). By improving and applying BAS, the optimal heading angle can be searched by minimizing the aggregate cost functions. Using the backstepping method, the controller is designed in the linear form and with constant control parameters. The control parameters are optimized through the BAS, such that the optimized control performance is achieved. Compared with the existing work, the novelties are summarized as follows.

1. The proposed guidance approach is totally described in mathematics without linguistic rules and grids. Compared with the routing results in refs. [3–5, 7, 10], the proposed scheme is easier for programming. Moreover, the proposed scheme considers the path following rather than the waypoint tracking, which has higher feasibility.

2. For the unmanned sailboat, the proposed guidance approach synthesizes the path following, the tacking and jibing maneuvers, and the collision avoidance of both dynamic and static obstacles altogether. Compared with the potential field methods in refs. [13–15], it requires no prior information of obstacles and wind. Compared with the path following principles in refs. [17–19], it has the better adaptability to diverse traffic conditions for collision avoidance.

3. The proposed controller requires no adaptive parameters, and its control gains can be trained offline. Compared with the adaptive controllers in refs. [18, 26, 28, 29], the computation burden is largely reduced. Compared with the PID control in refs. [15, 24, 25] and the robust control in refs. [27], the control performance can be optimized by modifying the BAS algorithm.

2. Modified BAS and FLS approximation

The BAS method is a meta-heuristic optimization algorithm mimicking the foraging behavior of beetles, which was first presented in ref. [30]. For a cost function of $F(x) = f(x) + \lambda \sum_{j=1}^k h_j(x)$, the goal is to minimize $F(x)$ by seeking the states x in k inequality constraints $g_j(x) \leq 0$, where λ is a very large positive constant and $h_j(x)$ is the penalty function described as

$$h_j(x) = \begin{cases} 1, & g_j(x) > 0 \\ 0, & g_j(x) \leq 0 \end{cases}$$

The current searching step is uniformly marked with a superscript t . Then, define x_r and x_l as searching states at the right and left antennae respectively, which have the form of

$$\begin{cases} x_r = x^t + d^t \vec{b} \\ x_l = x^t - d^t \vec{b} \end{cases} \tag{1}$$

where d^t is the current searching length and \vec{b} is a random direction vector with the identical length of x . Then, the states in the next searching step is determined as

$$x^{t+1} = x^t + \delta^t \vec{b} \text{sign}[F(x_l) - F(x_r)] \tag{2}$$

where $\delta^t = c_0 d^t$ with $0 < c_0 < 1$ is the moving length. Let $d^{t+1} = c_1 d^t$ with $0 < c_1 < 1$ and $d^t > 0$. Then, the searching can be finished while d^{t+1} is less than a preset positive threshold.

In the above customary BAS method proposed by ref. [30], we note a problem that x^{t+1} may be worse than x^t as it was only selected between x_r and x_l . To improve the searching performance, we can modify (2) as

$$x^{t+1} = \min \left\{ x^t, x^t + \delta^t \vec{b} \text{sign}[F(x_l) - F(x_r)] \right\} \tag{3}$$

This is referred to as “modified BAS”.

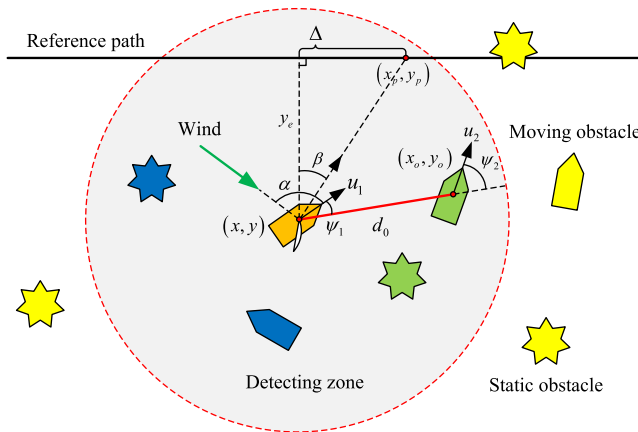


Figure 1. Illustration of variables and navigation tasks.

As was widely used in adaptive fuzzy control, any continuous nonlinear function in a compact set can be expressed by a FLS, namely

$$f_1(x) = W^T \varphi(x) + \varepsilon(x) \tag{4}$$

where $f_1(x)$ is the 1-dimensional nonlinear function defined in $x \in \Omega_x = \{x | x^T x \leq \Delta_x\}$, W is the constant vector of fuzzy weights, and $\varphi(x)$ is the vector of basis functions satisfying $\|\varphi(x)\| < 1$. $\varepsilon(x)$ is the approximation error bounded by $|\varepsilon(x)| < \bar{\varepsilon}$, and $\bar{\varepsilon}$ can be tuned to an arbitrarily small value by selecting appropriate W and $\varphi(x)$.

3. Guidance

The proposed guidance principle should reconcile tacking and jibing maneuver, path following and collision avoidance of unmanned sailboats. Here, we set a circular detecting zone of the unmanned sailboat with its planar position as the circle centre, which implies the detecting ability of apparatuses such as the radar and the sonar. Only the obstacles within the detecting zone is addressed. Corresponding to different navigation tasks, four cost functions were fabricated and then synthesized. Illustration of variables and navigation tasks is shown in Fig. 1. It should be noted that the heading direction of the sailboat therein only exhibits one of possible reference heading directions, where its real heading angle marked as ψ is not shown.

3.1. Collision avoidance

The sway speeds are omitted. If the sailboat has the reference heading direction in Fig. 1 and the reference heading angle is denoted as ψ_d , it will have the surge speed u_1 according to the speed polar diagram and the included angle towards the selected obstacle at (x_o, y_o) marked as ψ_1 , which is calculated by

$$\psi_1 = \arctan\left(\frac{y_o - y}{x_o - x}\right) + 90^\circ \times (1 - \text{sign}(x_o - x)) \times \text{sign}(y_o - y) - \psi_d \tag{5}$$

The sign function in (5) can guarantee that the bearing angle of (x_o, y_o) is always located within $(-180^\circ, 180^\circ]$. By using the onboard sensing devices like radar, the obstacle can be detected to have the surge speed u_2 and the included angle away from the sailboat ψ_2 . The distance between the sailboat and the obstacle is calculated as $d_o = \sqrt{(x - x_o)^2 + (y - y_o)^2}$. According to geometry, the future distance d from now on and after Δt is calculated by

$$d^2 = (d_0 - a_1 \Delta t)^2 + a_2^2 \Delta t^2 \tag{6}$$

where it has $a_1 = u_1 \cos(\psi_1) - u_2 \cos(\psi_2)$ and $a_2 = u_1 \sin(\psi_1) - u_2 \sin(\psi_2)$. The smallest d which is known as DCPA and marked as D_{CPA} , occurs at the TCPA which is marked as T_{CPA} , namely $\Delta t = T_{CPA}$. According to (6), it yields

$$T_{CPA} = \frac{d_0 a_1}{a_1^2 + a_2^2} \tag{7}$$

By substituting (7)–(6), it obtains

$$D_{CPA} = \frac{d_0 a_2}{\sqrt{a_1^2 + a_2^2}} \tag{8}$$

All the obstacles within the detecting zone should be evaluated through (7) and (8). The obstacles with $T_{CPA} \leq 0$ (i.e. blue obstacles in Fig. 1) should be exempted at first, and only the obstacles with $T_{CPA} > 0$ (i.e. green obstacles in Fig. 1) are considered. Assuming there are totally n obstacles with $T_{CPA} > 0$ and the concerned obstacle is marked with the superscript i , the cost function is fabricated as

$$f_1(\psi_d) = \sum_{i=1}^n \frac{\bar{d}(u_2^i)}{D_{CPA}^i} \tag{9}$$

where $\bar{d}(u_2^i)$ is the dead-zone operator designed as

$$\bar{d}(u_2^i) = \begin{cases} k_1 |u_2^i|, & |u_2^i| > \bar{u}_2 \\ k_1 \bar{u}_2, & |u_2^i| \leq \bar{u}_2 \end{cases}$$

where k_1 and \bar{u}_2 are positive constants.

3.2. Path following

Path following is the radical navigation goal of the unmanned sailboat. As shown in Fig. 1, LOS guidance is adopted here. A fixed look-forward distance Δ is put along the reference path from the foot of the perpendicular, which gets the target point (x_p, y_p) . Then, the reference heading angle of path following can be rendered as

$$\psi_{pf} = \arctan\left(\frac{y_p - y}{x_p - x}\right) + 90^\circ \times (1 - \text{sign}(x_p - x)) \times \text{sign}(y_p - y) \tag{10}$$

Similar with (5), the sign function in (10) can also ensure that $\psi_{pf} \in (-180^\circ, 180^\circ]$. The reference path is switched while the foot of the perpendicular reaches the next waypoint.

It is clear that if ψ is located within the zone of β , path following can still be achieved. If ψ is located within the zone of $180^\circ - \beta$, path following will be discounted and even cannot be achieved. In other situations, the sailboat will back off, which is unacceptable. Thus, while the sailboat is located in the right of the reference path (namely the situation in Fig. 1), the cost function is fabricated as

$$f_2(\psi_d) = \begin{cases} k_2(\psi_{pf} - \psi_d), & \psi_d \in [\psi_{pf} - \beta, \psi_{pf}] \\ g_2(|y_e|) \times (\psi_d - \psi_{pf}), & \psi_d \in (\psi_{pf}, \psi_{pf} + 180^\circ - \beta) \\ +\infty, & \text{otherwise} \end{cases} \tag{11}$$

While the sailboat is located in the left of the reference path, the cost function is rewritten as

$$f_2(\psi_d) = \begin{cases} k_2(\psi_d - \psi_{pf}), & \psi_d \in [\psi_{pf}, \psi_{pf} + \beta] \\ g_2(|y_e|) \times (\psi_{pf} - \psi_d), & \psi_d \in [\psi_{pf} - 180^\circ + \beta, \psi_{pf}] \\ +\infty, & \text{otherwise} \end{cases} \tag{12}$$

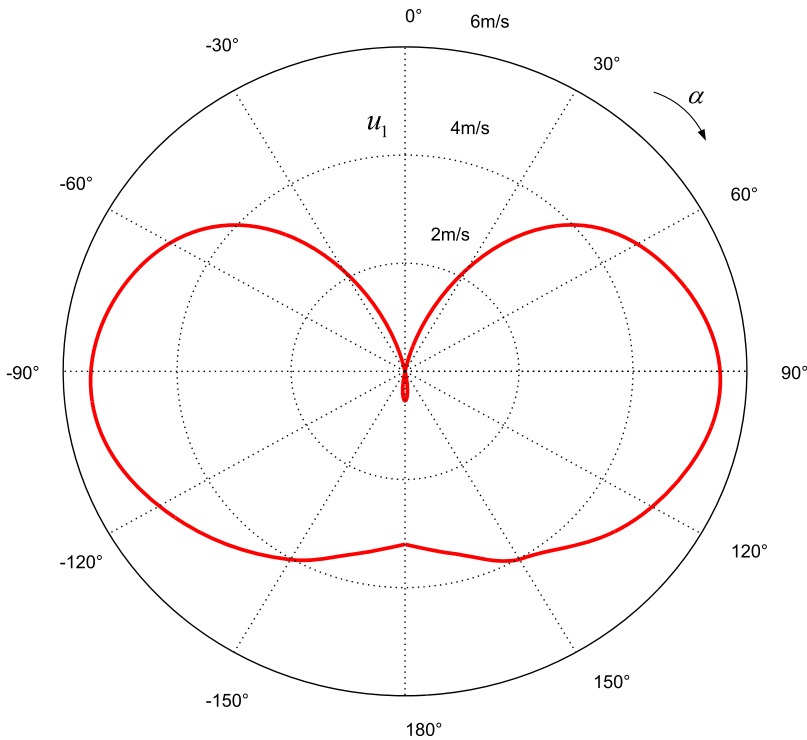


Figure 2. Speed polar diagram of a sailboat.

where k_2 is a positive constant, y_e is the cross-tracking error, and $g_2(|y_e|)$ is a dead-zone operator described as

$$g_2(|y_e|) = \begin{cases} k_2, & |y_e| < \bar{y} \\ \frac{k_2}{\bar{y}}|y_e|, & |y_e| \geq \bar{y} \end{cases} \tag{13}$$

where \bar{y} is a positive threshold. This suggests that sailing off course is acceptable while $|y_e|$ is small.

3.3. Speed loss

In the steady wind, the relationship between u_1 and α in Fig. 1 can be depicted by the speed polar diagram, which has the shape like an apple. Figure 2 gives an example. It is clear in Fig. 2 that the curve of u_1 is symmetric for $\alpha \in [-180^\circ, 0^\circ]$ and $\alpha \in [0^\circ, 180^\circ]$, and u_1 has a maximum value marked as \bar{u}_1 .

To guarantee existence of u_1 , the cost function of speed loss is constructed as

$$f_3(\psi_d) = k_3 \frac{\bar{u}_1}{|u_1|} \tag{14}$$

where k_3 is a tuning parameter.

3.4. Course loss

Large switching of ψ_d will lead to speed loss and deterioration of control effect. As the BAS algorithm is carried out step by step, the calculation of ψ_d must be discrete in the proposed scheme. Complying with the actual operational nature of the processor, it is presumed that the calculation period is a constant t_s . The current instant can be expressed by $t = i * t_s + t_0$, where the integer i is the current accumulative

calculation time and t_0 is the initial calculation instant. Then, the last calculation instant can be expressed as $t - t_s$ or $(i - 1) * t_s + t_0$. The cost function of course loss is fabricated as

$$f_4(\psi_d) = k_4|\psi_d - \psi(t - t_s)| \tag{15}$$

where k_4 is a positive tuning parameter.

3.5. Synthesis and optimization

The synthesized cost function is fabricated as

$$F(\psi_d) = f_1(\psi_d) + f_2(\psi_d) + f_3(\psi_d) + f_4(\psi_d) \tag{16}$$

Then, the guidance problem becomes the 1-dimensional BAS optimization of (16) by using (1)–(3). According to (2), x^1 is assigned as $\psi(t - t_s)$. By assigning appropriate values to d^1 , c_0 and c_1 , the ψ_d achieving the smallest $F(\psi_d)$ can be found at t .

Remark 1. The proposed scheme did not consider the collision avoidance regulations at sea, which is referred to as the COLREGs rules enacted by the international maritime organization (IMO). The COLREGs have stipulated the corresponding responses of the sailboat to different kinds of coming ships. For example, the sailboat will stand on for a power-driven ship in any case, but may give way for another coming sailboat. Thus, the involvement of the COLREGs demands the identification mechanism at first. Moreover, the coming ship may not abide by the COLREGs. In such cases, the proposed scheme is more advantageous for its initiative to avoid collision.

Remark 2. In the proposed guidance scheme, the selection of tuning parameters $k_1 \sim k_4$ depends on the actual needs of the current traffic condition. For example, if the sailboat is sailing in the crowded waters, k_1 should be tuned up to increase its ability of collision avoidance; if the sailboat is sailing in the open waters, k_2 should be tuned up to facilitate the path following; if the sailboat is sailing with the weak wind, k_3 and k_4 should be tuned up to prevent from the speed loss.

4. Control design

4.1. Linear backstepping controller

According to refs. [19, 26], the heading angle of an unmanned sailboat can be controlled through

$$\begin{cases} \dot{\psi} = r \\ \dot{r} = \frac{N_S}{m_r} + \frac{N_H}{m_r} + \frac{N_R}{m_r} - \frac{d_r}{m_r}|r|r \\ \dot{\delta} = -\frac{1}{T}\delta + \frac{1}{T}\delta_c \end{cases} \tag{17}$$

where r is the yaw rate, δ is the real rudder angle limited in $[-35^\circ, +35^\circ]$, and δ_c is the command rudder angle treated as the control input. N_S denotes the torque generated by the sail, which is associated with the true wind and the sheeting angle of the sail. $N_H = N_{ur}u_1r + N_r r$ denotes the torque generated by the hull, where N_{ur} and N_r are hydrodynamic derivatives. d_r is the damping coefficient in the yaw motion, and T is the time constant. N_R is treated as the dominant torque generated by the rudder, which is written as

$$N_R = \frac{1}{2}\rho_w A f_\alpha u_1^2 |x_r| \sin(\delta) \tag{18}$$

where ρ_w is the density of water, A is the rudder area, f_α is the slope of lift at $\delta = 0$, and x_r is the distance from the rudder centroid to the gravity center of the whole sailboat. For simplicity, (18) is reexpressed as $N_R = c_r m_r \sin(\delta)$. It is clear that $c_r > 0$ and is bounded.

Table I. Pseudo codes of the proposed scheme.

```

Initialize  $x, y, \psi, r$  of the sailboat
for the computing time from  $i = 1$  to  $i = N$ 
do
    detect  $(x_o, y_o)$  and  $u_2$  of obstacles within the detecting zone
    assign  $x^1 = \psi(t_0 + (i - 1) * t_s)$  and  $t = 1$ 
    while  $d^t$  larger than the searching threshold
    do
        calculate  $x_r$  and  $x_l$  from (1)
        calculate  $T_{CPA}$  from (7) and filter out  $T_{CPA} \leq 0$ 
        calculate  $F(x_l)$  and  $F(x_r)$  from (16)
        calculate  $x^{t+1}$  from (3)
        update  $d^{t+1}$  and let  $t = t + 1$ 
    end while
    assign  $\psi_d(t_0 + i * t_s) = x^t$ 
    calculate  $\delta_c(t_0 + i * t_s)$  from (22)
    execute  $\delta_c(t_0 + i * t_s)$  in the sailboat which can be described by (17)
end for
    
```

Denote the tracking error of ψ as $\psi_e = \psi - \psi_d$. According to the backstepping method, the virtual control law of r is designed as $\alpha_r = -k_\psi \psi_e$, where k_ψ is a positive tuning parameter. Denote the tracking error of r as $r_e = r - \alpha_r$. Differentiating ψ_e along with (17) and α_r , it renders

$$\dot{\psi}_e = -k_\psi \psi_e + r_e - \dot{\psi}_d \tag{19}$$

By using (4), it can be expressed that $(N_H + N_S - d_r|r|)/m_r - \dot{\alpha}_r = W^T \varphi(u_1, r) + \varepsilon$. Invoking (17), it gives $\dot{r}_e = c_r \sin(\delta) + W^T \varphi + \varepsilon$. According to backstepping, the virtual control law of $\sin(\delta)$ is designed as $\alpha_{\sin \delta} = -k_r r_e$, where k_r is a positive tuning parameter. Denote the tracking error of $\sin(\delta)$ as $s_e = \sin(\delta) - \alpha_{\sin \delta}$. r_e is further transformed to

$$\dot{r}_e = -k_r c_r r_e + c_r s_e + W^T \varphi + \varepsilon \tag{20}$$

Differentiating s_e along with (17), it renders

$$\dot{s}_e = \cos(\delta) \dot{\delta} - \dot{\alpha}_{\sin \delta} = \frac{\cos(\delta)}{T} (\delta_c - \delta) - \dot{\alpha}_{\sin \delta} \tag{21}$$

To mediate the convergence of s_e , the real control law of δ_c is designed as $\delta_c = -k_\delta T s_e / \cos(\delta) + \delta$, where k_δ is a positive tuning parameter. Define $k'_\delta = k_\delta T$. By involving the definitions of s_e and r_e , δ_c is further transformed to

$$\delta_c = -k'_\delta \tan(\delta) - \frac{k'_\delta k_r}{\cos(\delta)} r - \frac{k'_\delta k_r k_\psi}{\cos(\delta)} \psi_e + \delta \tag{22}$$

By incorporating δ_c in (21), it renders

$$\dot{s}_e = -k_\delta s_e - \dot{\alpha}_{\sin \delta} \tag{23}$$

In nautical practice, the work of the proposed scheme is demonstrated in the pseudo codes of Table I. It is shown that two loops are nested. The inner loop takes the BAS optimization and searches ψ_d , the outer one undertakes the controller and generates δ_c . In the proposed scheme, both the guidance signal ψ_d and the control signal δ_c are calculated step by step with a constant calculation period t_s . Because ψ_d is updated through the BAS algorithm in each step, its continuity is not guaranteed. Because $\psi_d \in (-180^\circ, 180^\circ]$ and $\dot{\psi}_d \approx [\psi_d(t) - \psi_d(t - t_s)]/t_s$, it is feasible to ensure $\psi \rightarrow \psi_d$ by using the proposed controller.

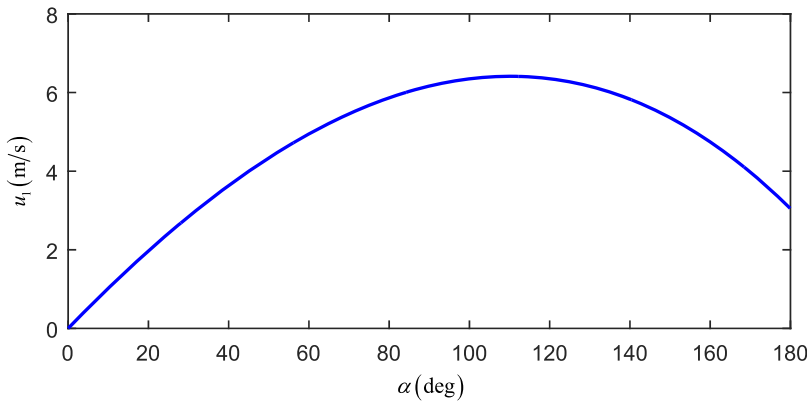


Figure 3. Curve of α to u_1 .

4.2. Stability analysis

The proposed control scheme can be concluded as the following theorem.

Theorem 4.1. *For the horizontal motions of a sailboat described by (17), the linear backstepping controller fabricated in (22) can ensure the semi-global uniform ultimate boundedness (SGUUB) of all the tracking errors. By optimizing the tuning parameters of k_ψ , k_r and k_δ , the balance between the tracking accuracy and the energy cost can be achieved.*

Proof: Select a Lyapunov candidate as $V = (\psi_e^2 + r_e^2 + s_e^2)/2$. Note the following inequality

$$W^T \varphi + \varepsilon \leq \theta(\|\varphi\| + 1) \leq 2\theta \tag{24}$$

where $\theta = \max\{\|W\|, \bar{\varepsilon}\}$. By using the Young's inequality and differentiating V along with (19), (20), (23) and (24), it renders

$$\begin{aligned} \dot{V} &= \psi_e \dot{\psi}_e + r_e \dot{r}_e + s_e \dot{s}_e \\ &\leq -(k_\psi - 1)\psi_e^2 - \left(k_r c_r - \frac{c_r^2}{2} - \frac{3}{2}\right)r_e^2 - (k_\delta - 1)s_e^2 + \frac{1}{2}\dot{\psi}_d^2 + \frac{1}{2}\theta^2 + \frac{1}{2}\dot{\alpha}_{\sin \delta}^2 \end{aligned} \tag{25}$$

As ψ and r are limited in the real environment, it is tenable to define $\varrho = (\dot{\psi}_d^2 + \theta^2 + \dot{\alpha}_{\sin \delta}^2)/2$ bounded by $\bar{\varrho}$. Select $k_\psi > 1$, $k_r > c_r/2 + 3/(2c_r)$ and $k_\delta > T$. Let $\eta = \min\{2k_\psi - 2, 2k_r c_r - c_r^2 - 3, 2k_\delta - 2\}$. Then, (25) can be transformed to $\dot{V} \leq -\eta V + \bar{\varrho}$, which further renders

$$V(t) \leq V(0)e^{-\eta t} + (1 - e^{-\eta t})\frac{\bar{\varrho}}{\eta} \tag{26}$$

which implies that $V(t)$ is ultimately bounded by $\bar{\varrho}/\eta$. The proof is completed.

Remark 3. It is shown in (22) that only three tuning parameters are required in the controller. Compared with the adaptive control of sailboats, such as [18, 28], the neural networks with adaptive laws are no longer required, and the computational simplicity is guaranteed. To refrain from manual intervention, the BAS-based parameter optimization is proposed in the next section.

4.3. BAS-based parameter optimization

The optimization objective is to achieve the satisfactory tracking accuracy as little energy cost as possible. By using the modified BAS algorithm, k'_δ , k_r and k_ψ are determined. Synthesizing the tracking error

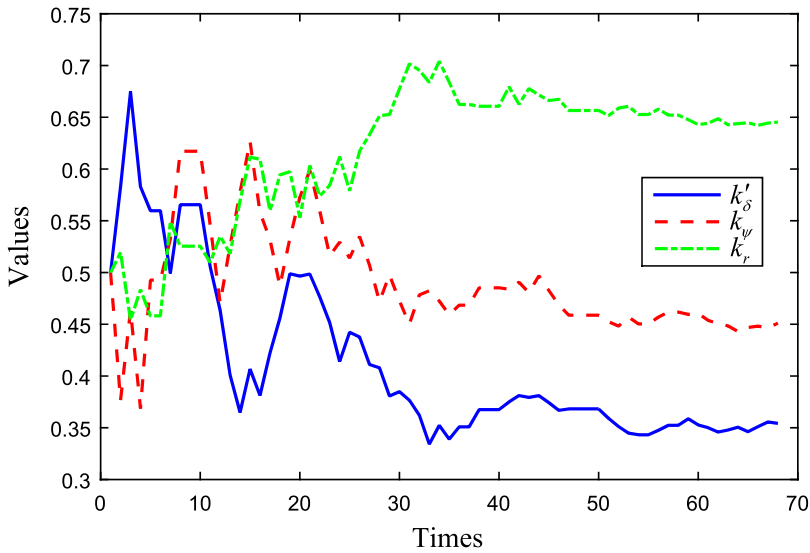


Figure 4. Recursive update of x^t .

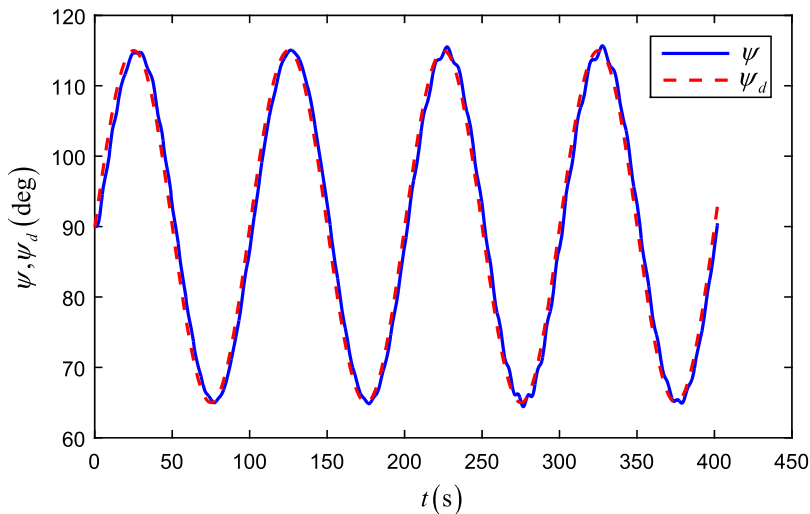


Figure 5. Evolution of ψ and ψ_d in BAS optimization.

and the energy cost together, the cost function is fabricated as

$$F_c(k_\psi, k_r, k_\delta) = \int_{t_1}^{t_2} \alpha_1 \psi_e^2 + (1 - \alpha_1) \delta^2 dt \tag{27}$$

where $\alpha_1 \in [0, 1]$ is the weight to reconcile the amplitudes between ψ_e and δ . t_1 and t_2 are the initial and the ending instants of the recording time, respectively.

The parameter optimization process can follow the procedure that: (1) preset the values of k_δ^t , k_r and k_ψ ; (2) steer the sailboat to a stable navigation condition, namely close to the reference direction and not in a turbulent wind; (3) set $x^1 = [k_\delta^t, k_\psi, k_r]^T$, d^1 , c_0 , c_1 , α_1 and fixed $t_2 - t_1$; (4) use BAS and calculate F_c of x_l , x^t and x_r at the following three time intervals of $t_2 - t_1$; (5) redetermine the values of k_δ^t , k_r and k_ψ .

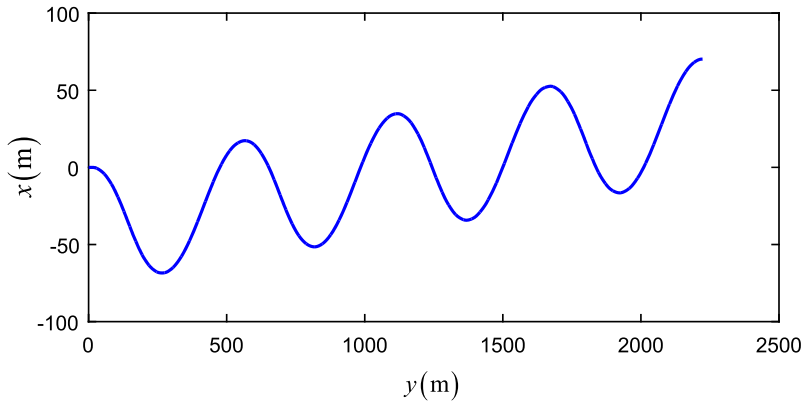


Figure 6. Trajectory of sailboat in BAS optimization.

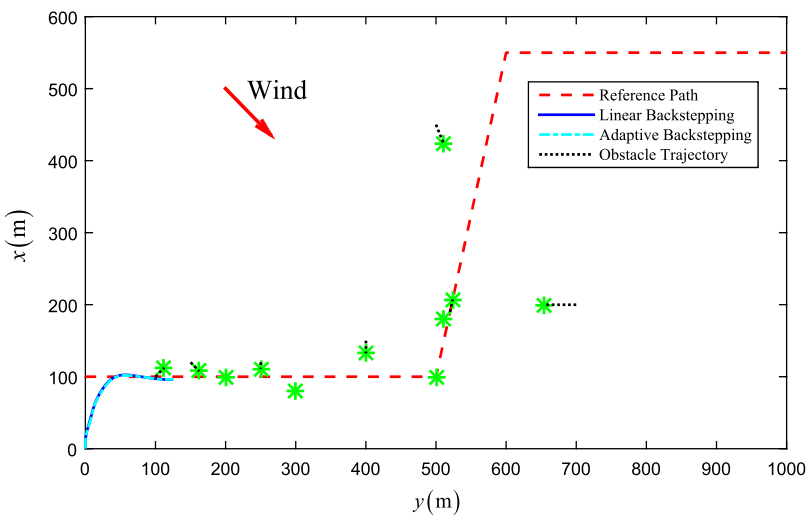


Figure 7. Trajectory of sailboat at 35 s.

5. Simulation

A 1.3-m sailboat is chosen to be the experimental objective, which has $m_r = 50.5$, $N_{ur} = -2$, $N_r = -10$, $d_r = 5$, $f_\alpha = 2.4$, $A = 0.1 \text{ m}^2$, $x_r = -0.3 \text{ m}$ and $T = 5$. Wind is set with the Beaufort wind scale of No.5, which is 135° right to the north. According the speed polar diagram, the relationship between α and u_1 can be described by a polynomial as $u_1(\alpha) = -0.17|\alpha|^3 - 1.08\alpha^2 + 6.04|\alpha|$. The curve of $\alpha \in [0^\circ, 180^\circ]$ to u_1 is shown in Fig. 3, which is symmetric along the u_1 axis.

The first numerical experiment is to determine the optimized parameters in (22). The optimization process follows the procedures in Section 4.3. The initial states of the sailboat are set as $[x(0), y(0), \psi(0)] = [0 \text{ m}, 0 \text{ m}, 90^\circ]$, $r(0) = 0^\circ/\text{s}$ and $\delta = 0^\circ$. α_1 in (27) is set as 0.8. A sinusoidal reference signal of ψ_d is given along time, namely $\psi_d = \pi/2 + 5\pi/36 \sin(\pi t/50)$. The initial values of three parameters are set as $k_\delta = 0.5$, $k_\psi = 0.5$ and $k_r = 0.5$. According to the modified BAS, set $d^1 = 0.18$, $\delta^t = 0.15$, $c_1 = 0.95$, the final threshold of d^t as 0.006 and $t_2 - t_1$ in (27) as 2 s. Thus, x^t , x_t , and x_r are tested in every 2 s. x^{t+1} is determined after every 6 s.

The optimization process is shown in Fig. 4. After 67 times iteration, optimization is over and it finally renders $k_\delta = 0.36$, $k_\psi = 0.64$ and $k_r = 0.44$. Along with the optimization, the tracking performance is

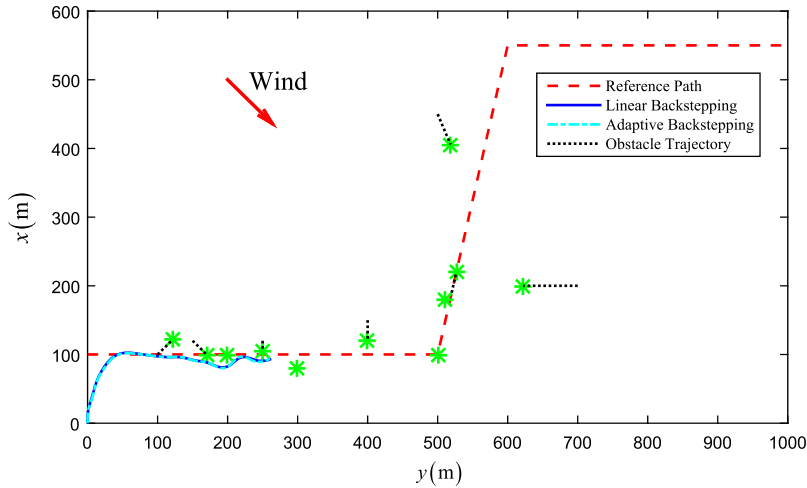


Figure 8. Trajectory of sailboat at 60 s.

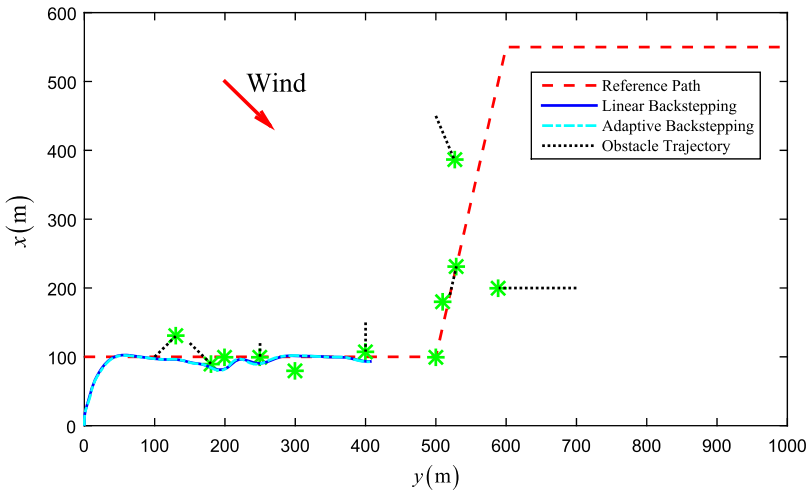


Figure 9. Trajectory of sailboat at 85 s.

shown in Fig. 5. It is shown that tracking accuracy is gradually enhanced along with the optimization of control parameters. The trajectory of the sailboat is shown in Fig. 6. A sinusoidal trajectory is achieved.

The second numerical experiment is to verify the effectiveness of the proposed guidance scheme and the superior control performance of the linear backstepping controller. In this experiment, four waypoints are set, namely $(x_1, y_1) = (100 \text{ m}, 0 \text{ m})$, $(x_2, y_2) = (100 \text{ m}, 500 \text{ m})$, $(x_3, y_3) = (550 \text{ m}, 600 \text{ m})$, and $(x_4, y_4) = (550 \text{ m}, 1000 \text{ m})$. The reference path is generated by connecting adjacent waypoints. To imitate the complicated traffic situations, 11 obstacles are set with initial positions and heading angles as $(100 \text{ m}, 100 \text{ m}, 45^\circ)$, $(100 \text{ m}, 200 \text{ m}, 0^\circ)$, $(120 \text{ m}, 150 \text{ m}, 135^\circ)$, $(120 \text{ m}, 250 \text{ m}, -180^\circ)$, $(80 \text{ m}, 300 \text{ m}, 0^\circ)$, $(150 \text{ m}, 400 \text{ m}, -180^\circ)$, $(100 \text{ m}, 500 \text{ m}, 0^\circ)$, $(200 \text{ m}, 700 \text{ m}, -90^\circ)$, $(190 \text{ m}, 520 \text{ m}, 12.5^\circ)$, $(180 \text{ m}, 510 \text{ m}, 0^\circ)$, and $(450 \text{ m}, 500 \text{ m}, 157.5^\circ)$. Moving speeds u_2 of these obstacles are set as 0.5, 0, 0.5, 0.25, 0, 0.5, 0, 1.3, 0.5, 0 and 0.8 m/s. The initial states of the sailboat is set as $(x(0), y(0), \psi(0)) = (0 \text{ m}, 0 \text{ m}, 0^\circ)$, $r(0) = 0$ and $\delta(0) = 0$. According to the proposed guidance principle, the detecting zone is set with the radius of 50 m, and let $k_1 = 1000$, $\bar{u}_2 = 1 \text{ m/s}$, $k_2 = 100$, $\bar{y} = 10 \text{ m}$,

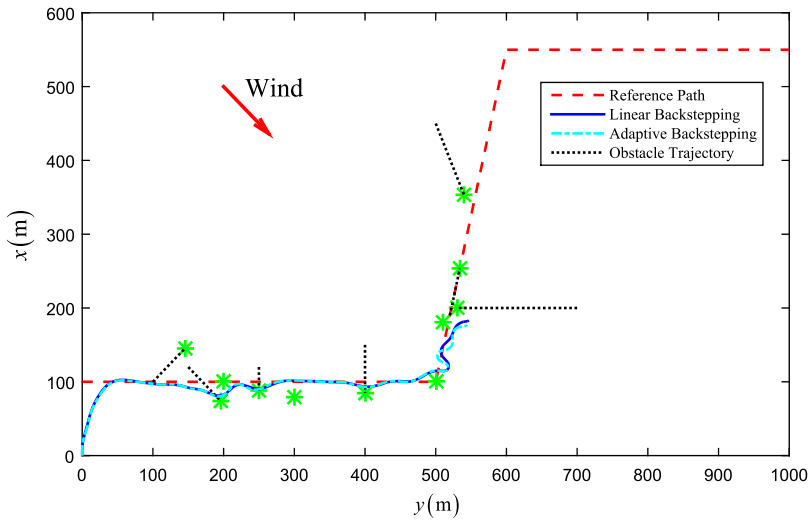


Figure 10. Trajectory of sailboat at 130 s.

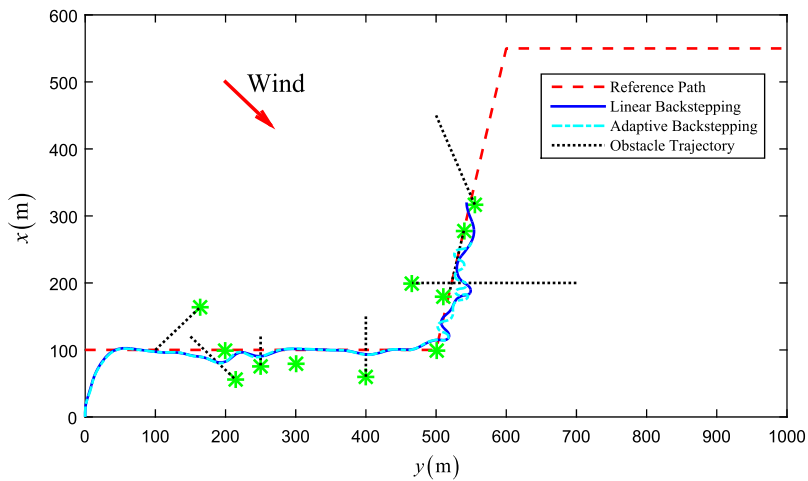


Figure 11. Trajectory of sailboat at 180 s.

$k_3 = 100$, $\bar{u}_1 = 6$ m/s and $k_4 = 50$. By using the optimized parameters $k'_\delta = 1.10$, $k_\psi = 0.58$ and $k_r = 0.43$, the guidance principle with the controller in (22) is marked as “Linear Backstepping”. To verify the superiority, the adaptive controller in ref. [18] is set as the comparison, which is marked as “Adaptive Backstepping”. According to direct adaptive control, the controller of comparison is fabricated as

$$\delta_c = -k'_\delta \tan(\delta) - \frac{k'_\delta k_r}{\cos(\delta)} r - \frac{k'_\delta k_r k_\psi}{\cos(\delta)} \psi_e - \frac{k'_\delta \hat{W}^T \varphi}{\cos(\delta)} + \delta \tag{28}$$

where the adaptive law is designed as

$$\dot{\hat{W}} = \Gamma(\varphi(r - k_\psi \psi_e) - \sigma \hat{W}) \tag{29}$$

Then, simulation results are shown in the following figures.

Figures 7–13 show trajectories of the sailboat in some typical collision-avoidance situations under two control laws, for example, cross from left in Figs. 8 and 9, cross from right in Figs. 7 and 10, overtaking in Fig. 11 and head on in Fig. 12. It should be noted that the sailboat is not required to

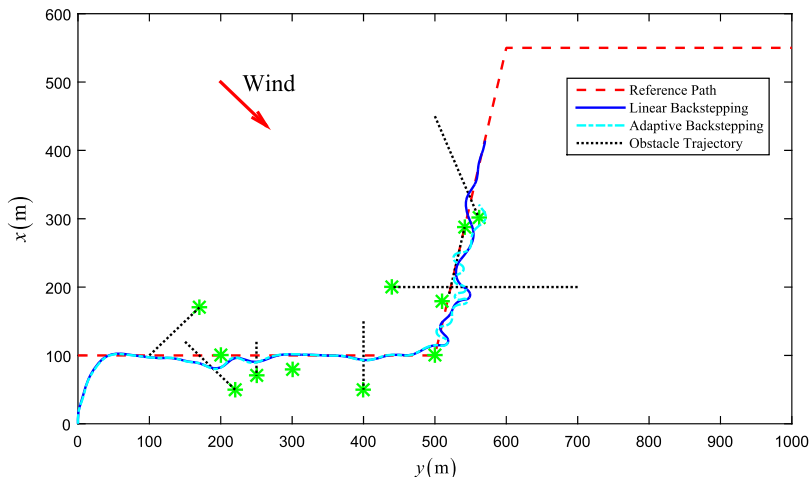


Figure 12. Trajectory of sailboat at 200 s.

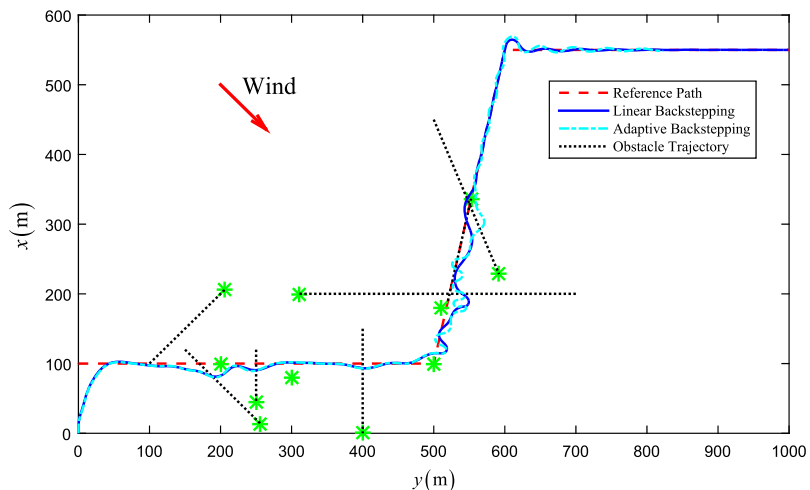


Figure 13. Trajectory of sailboat at 300 s.

obey the International Regulations for Preventing Collisions at Sea (COLREGS). It is clear in these figures that the sailboat successfully bypasses the obstacles and the safe distance is left for a 1.3 m sailboat. Effectiveness of the proposed BAS-based guidance is substantiated. Nevertheless, it is shown in Figs. 11 and 13 that “Adaptive Backstepping” has the significant trajectory fluctuation than “Linear Backstepping”. It implies that the adaptive term in (28) will degrade the stability and lead to the control inefficiency. Speeds of the sailboats under two controllers are shown in Fig. 14. Tracking errors and control inputs are shown in Figs. 15 and 16, respectively. Large deviations of these curves are shown in “Adaptive Backstepping”, which verifies the superiority of the proposed linear backstepping controller. Through the entire control voyage, F_c of “Linear Backstepping” and “Adaptive Backstepping” are 617.8 and 863.0, respectively. Optimized control performance is exhibited in “Linear Backstepping”. Figure 17 shows the direct adaptive law of \hat{W} in “Adaptive Backstepping”, where all the elements are bounded. With the simulation environmental configuration (CPU: Intel Core i7-10875H 2.3 GHz 2.3 GHz, RAM: 16.0 GB), it is tested that “Linear Backstepping” has the total computing time (TCT) of 126.89 s and the memory occupancy (MO) of 916460 kB, whereas “Adaptive Backstepping” has the TCT of 139.28 s and the MO of 1009996 kB. The less computation burden is verified in the proposed scheme.

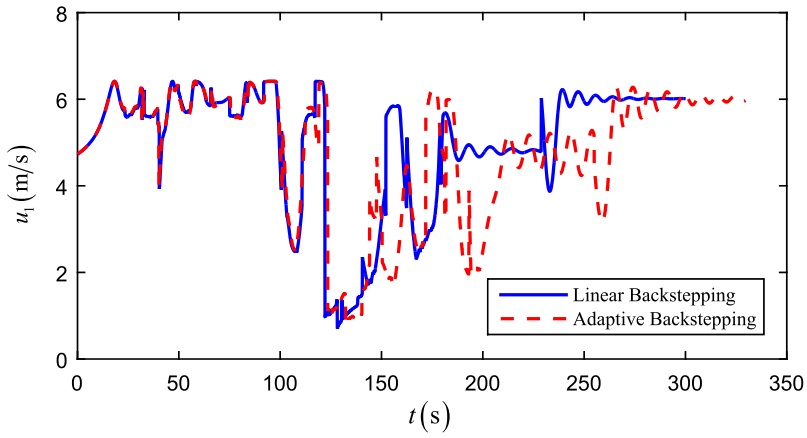


Figure 14. Speed of sailboat.

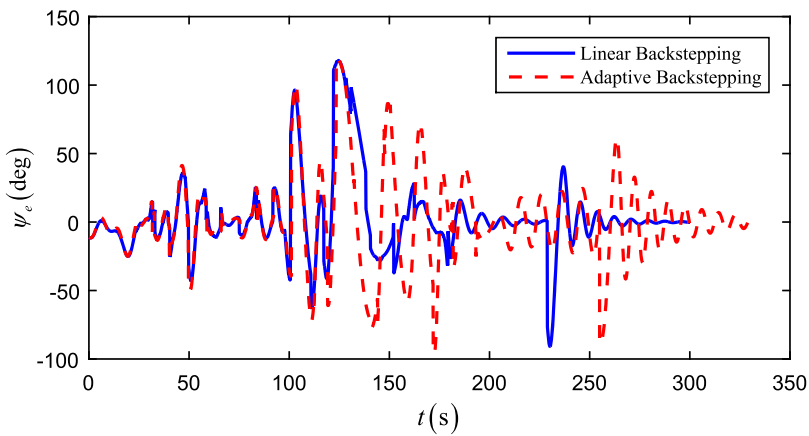


Figure 15. Tracking error ψ_e of sailboat.

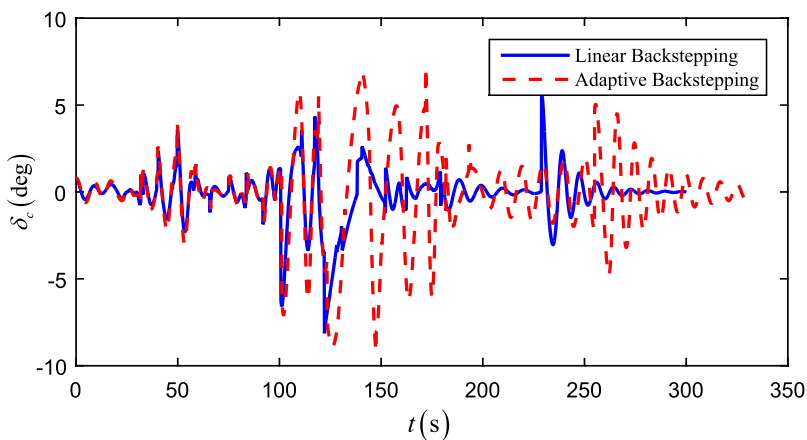


Figure 16. Control inputs.

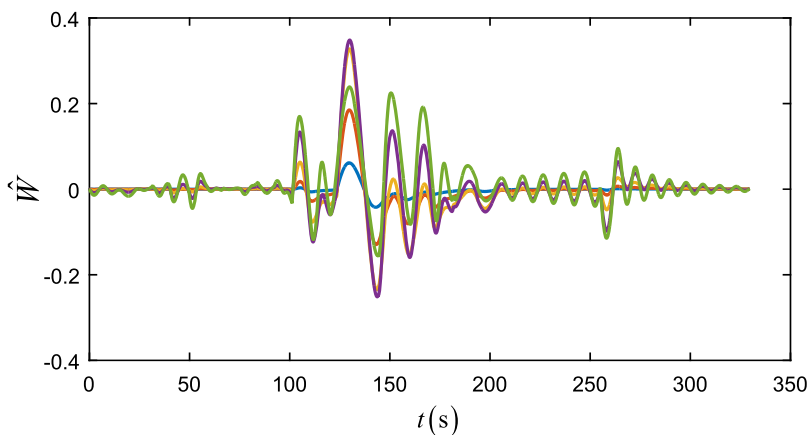


Figure 17. Adaptive law of \hat{W} in “Adaptive Backstepping”.

6. Conclusion

Based on the modified BAS optimization algorithm, a guidance principle with a linear backstepping controller is proposed for the unmanned sailboat, which synthesizes the tasks of path following, collision avoidance and the characteristic sailboat maneuvers together. By using the bounded property of fuzzy basis functions, the linear backstepping controller is fabricated in a succinct way. The parameters of the linear backstepping controller are determined by using the BAS optimization, so as to ensure the optimized control performance, namely satisfactory tracking accuracy with less energy cost. Simulation verifies the effectiveness of the proposed guidance and control strategies. In the future work, a real sea trial of the sailboat should be carried out. Besides, more abilities can be added to the guidance, such as station keeping and zone scanning.

Author contributions. Yingjie Deng: Data curation, Writing. Tao Ni: Methodology, Software. Zhuxin Zhu: Conceptualization, Supervision. Jianwei Wang: Visualization, Investigation.

Financial support. This work is partially supported by the Natural Science Foundation of China (No.52101375), the Hebei Province Natural Science Fund (No.E2021203142), the Joint Funds of the National Natural Science Foundation of China (No.U20A20332), and the Key Research and Development Project of Hebei Province (No.21351802D).

Conflicts of interest. The authors declare that they have no known competing financial interests or personal relationships that could have appeared to influence the work reported in this paper.

References

- [1] P. F. Rynne and K. D. von Ellenrieder, “Unmanned autonomous sailing: Current status and future role in sustained ocean observations,” *Mar. Technol. Soc. J.* **43**(1), 21–30 (2009).
- [2] M. F. Silva, A. Friebe, B. Malheiro, P. Guedes, P. Ferreira and M. Waller, “Rigid wing sailboats: A state of the art survey,” *Ocean Eng.* **187**, 106150 (2019).
- [3] H. Erckens, G.-A. Büsser, C. Pradalier and R. Y. Siegwart, “Navigation strategy and trajectory following controller for an autonomous sailing vessel,” *IEEE Robot. Autom. Mag.* **17**(1), 45–54 (2010).
- [4] Langbein J., Stelzer R. and Frühwirth T., “A Rule-based Approach to Long-Term Routing for Autonomous Sailboats,” **In: Proceedings of 4th International Robotic Sailing Conference**, Lübeck, Germany (2011) pp. 195–204.
- [5] M. Zyczkowski and R. Szlapczynski, “Collision risk-informed weather routing for sailboats,” *Reliab. Eng. Syst. Safety* **232**, 109015 (2022). doi: [10.1016/j.ress.2022.109015](https://doi.org/10.1016/j.ress.2022.109015).
- [6] J. C. Alves and N. A. Cruz, “A Mission Programming System for an Autonomous Sailboat,” **In: Oceans. St. John’s (IEEE, Canada, 2014)** pp. 1–7.
- [7] M. Zyczkowski, P. Krata and R. Szlapczyński, “Multi-objective weather routing of sailboats considering wave resistance,” *Pol. Marit. Res.* **97**(25), 4–12 (2018).

- [8] T. Zvyagina and P. Zvyagin, “A model of multi-objective route optimization for a vessel in drifting ice,” *Reliab. Eng. Syst. Safety* **218**, 108147 (2022).
- [9] J. Szlapczynska, “Multi-objective weather routing with customised criteria and constraints,” *J. Navig.* **68**(2), 338–354 (2015).
- [10] TynanD., “An aAttractor/Rrepellor Aapproach to Aautonomous Ssailboat Nnavigation,” **In: Proceedings of the 10th International Robotic Sailing Conference**, Horten, Norway (2017) pp. 69–79.
- [11] C. Chen, X. Chen, F. Ma, X. Zhang and J. Wang, “A knowledge-free path planning approach for smart ships based on reinforcement learning,” *Ocean Eng.* **189**, 106299 (2019).
- [12] R. Stelzer and T. Pröll, “Autonomous sailboat navigation for short course racing,” *Robot. Auton. Syst.* **56**(7), 604–614 (2008).
- [13] C. Pêtrès, M. A. Romero-Ramirez and F. Plumet, “A potential field approach for reactive navigation of autonomous sailboats,” *Robot. Auton. Syst.* **60**(12), 1520–1527 (2012).
- [14] F. Plumet, C. Pêtrès, M. A. Romero-Ramirez, B. Gas and S. H. Ieng, “Toward an autonomous sailing boat,” *IEEE J. Oceanic Eng.* **40**(2), 397–407 (2015).
- [15] H. Saoud, M. D. Hua, F. Plumet and F. B. Amar, “Routing and Course Control of an Autonomous Sailboat,” **In: European Conference on Mobile Robots (ECMR)** (IEEE, 2015) pp. 1–6.
- [16] Less'ard-Springett J., Friebe A. and Gallic M. L., “Voter Bbased Ccontrol Ssystem for Ccollision Aavoidance and Ssailboat Nnavigation,” **In: Proceeding of 10th International Robotic Sailing Conference**, Horten, Norway (2017) pp. 57–68.
- [17] G. Elkaim and R. Kelbley, “Station Keeping and Segmented Trajectory Control of a Wind-Propelled Autonomous Catamaran,” **In: IEEE Conference on Decision and Control** (2006) pp. 2424–2429.
- [18] Y. Deng, X. Zhang and G. Zhang, “Line-of-sight-based guidance and adaptive neural path-following control for sailboats,” *IEEE J. Oceanic Eng.* **45**(4), 1177–1189 (2020).
- [19] Y. Deng, X. Zhang, G. Zhang and C. Huang, “Parallel guidance and event-triggered robust fuzzy control for path following of autonomous wing-sailed catamaran,” *Ocean Eng.* **190**, 106442 (2019).
- [20] G. Zhang, Y. Deng, W. Zhang and C. Huang, “Novel dvs guidance and path-following control for underactuated ships in presence of multiple static and moving obstacles,” *Ocean Eng.* **170**, 100–110 (2018).
- [21] S. Wang, Y. Zhang and L. Li, “A collision avoidance decision-making system for autonomous ship based on modified velocity obstacle method,” *Ocean Eng.* **215**, 107910 (2020).
- [22] M. Corno, S. Formentin and S. M. Savaresi, “Data-driven online speed optimization in autonomous sailboats,” *IEEE Trans. Intell. Transp.* **17**(3), 762–771 (2016).
- [23] R. Stelzer, T. Pröll and R. I. John, “Fuzzy Logic Control System for Autonomous Sailboats,” **In: IEEE International Fuzzy Systems Conference** (2007) pp. 1–6.
- [24] N. A. Cruz and J. C. Alves, “Auto-Heading Controller for an Autonomous Sailboat,” **In: OCEANS** (IEEE, 2010) pp. 1–6.
- [25] C. Viel, U. Vautier, J. Wan and L. Jaulin, “Position Keeping Control of an Autonomous Sailboat,” **In: IFAC PapersOnLine** (Elsevier, 2018) pp. 14–19.
- [26] L. Xiao, T. I. Fossen and J. Jouffroy, “Nonlinear Robust Heading Control for Sailing Yachts,” **In: 9th IFAC Conference on Manoeuvring and Control of Marine Craft** (IFAC, 2012) pp. 404–409.
- [27] L. Xiao and J. Jouffroy, “Modeling and nonlinear heading control of sailing yachts,” *IEEE J. Oceanic Eng.* **39**(2), 256–268 (2014).
- [28] Y. Deng, X. Zhang, Q. Zhang and Y. Hu, “Event-triggered composite adaptive fuzzy control of sailboat with heeling constraint,” *Ocean Eng.* **211**, 107627 (2020).
- [29] Y. Deng, Z. Zhang, M. Gong and T. Ni, “Event-triggered asymptotic tracking control of underactuated ships with prescribed performance,” *IEEE Trans. Intell. Transp.* **24**(1), 645–656 (2022). doi: [10.1109/tits.2022.3216808](https://doi.org/10.1109/tits.2022.3216808).
- [30] X. Jiang and S. Li, “Beetle antennae search without parameter tuning(bas-wpt) for multi-objective optimization (2017), *arXiv preprint*, vol. [arXiv:1711.02395](https://arxiv.org/abs/1711.02395).